

Layer by Layer, Patterned Valves Enable Programmable Soft Surfaces

JESSE T. GONZALEZ and SCOTT E. HUDSON, Carnegie Mellon University, USA



Fig. 1. Through a combination of bulk fabrication processes and layered assembly, we arrive at a composite material that contains both computational elements (a) and embedded, mechanical mesostructures. One such mesostructure is an electrostatic valve (b), which enables pneumatic control of soft surfaces (c). We refer to this particular composite (the electrostatic valve array) as *Stoma-Board*, an allusion to the pores in plant leaves (stomata) that regulate air exchange.

Programmable surfaces, which can be instructed to alter their shape or texture, may one day serve as a platform for tangible interfaces and adaptive environments. But so far, these structures have been constrained in scale by a challenging fabrication process, as the numerous constituent actuators must be built and assembled individually. We look towards emerging trends in mechanical engineering and consider an alternate framework — layer-driven design, which enables the production of dynamic, discretely-actuated surfaces at multiple scales. By centering the construction around patterning and stacking, forgoing individual assembly in favor of bulk processes such as photo-etching and laser cutting, we avoid the need for multiple manufacturing steps that are repeated for each of the many actuators that compose the surface. As an instance of this layer-driven model, we build an array of electrostatic valves, and use this composite material (which we refer to as *Stoma-Board*) to drive four types of pneumatic transducers. We also show how this technique may be readily industrialized, through integration with the highly mature and automated manufacturing processes of modern electronics.

CCS Concepts: • **Hardware** → PCB design and layout; • **Human-centered computing** → *Haptic devices; Interface design prototyping*; • **Computer systems organization** → *Robotics*.

Additional Key Words and Phrases: programmable materials, metamaterials, tangible interfaces, soft robotics

ACM Reference Format:

Jesse T. Gonzalez and Scott E. Hudson. 2022. Layer by Layer, Patterned Valves Enable Programmable Soft Surfaces. *Proc. ACM Interact. Mob. Wearable Ubiquitous Technol.* 6, 1, Article 12 (March 2022), 25 pages. <https://doi.org/10.1145/3517251>

1 INTRODUCTION

Every day, we interact with dozens of physical surfaces that are largely static. Forward-looking designers have perceived an opportunity in this space — anticipating a suite of tangible, shape-changing interfaces that are as mutable as their digital relatives [57]. But such surfaces, clearly, are far from commonplace today.

Authors' address: Jesse T. Gonzalez, jtgonzal@cs.cmu.edu; Scott E. Hudson, scott.hudson@cs.cmu.edu, Carnegie Mellon University, Pittsburgh, Pennsylvania, USA, 15213.

Permission to make digital or hard copies of part or all of this work for personal or classroom use is granted without fee provided that copies are not made or distributed for profit or commercial advantage and that copies bear this notice and the full citation on the first page. Copyrights for third-party components of this work must be honored. For all other uses, contact the owner/author(s).

© 2022 Copyright held by the owner/author(s).

2474-9567/2022/3-ART12

<https://doi.org/10.1145/3517251>

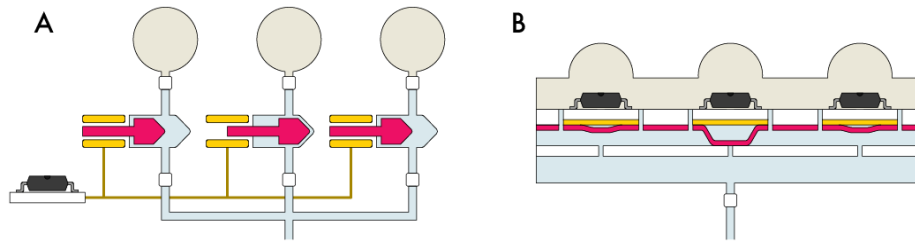


Fig. 2. A module-driven design (a), in the form of a solenoid array, is contrasted with a layer-driven design (b), in the form of an electrostatic valve array. Actuators in (a) are distinct mechanisms; actuators in (b) are cells in a common substrate. Communication in (a) is centralized (one-to-many); communication in (b) is distributed (neighbor-to-neighbor). Energy in (a) is transmitted via independent branches; energy in (b) is accessible through a global, unified reservoir.

The few existing objects that *do* adapt to our inputs (tactile displays¹, for instance) are specialized devices, only able to achieve a physical state change through the complex manipulation of multiple independent elements [13, 21]. This modular design, while workable in cost-agnostic settings, is limited in practice by a labor-intensive construction process [1]. If we are interested in making shape-shifting surfaces pervasive within our world, then this discretely-assembled machinery must be replaced with a more fabrication-friendly alternative.

Layered construction provides a solution. Among some mechanical engineers, there is an emerging migration from multi-piece mechanisms to cleverly-designed composites — soft and flexible structures that arise from the stacking of patterned films [40, 47]. In this paper, we adopt layer-driven design as a method for building programmable pneumatic surfaces that are inherently scalable. We introduce an electrostatic valve array (Figure 1), which we refer to as *Stoma-Board* — an allusion to the micro-scale pores (stomata) that regulate air intake from the surface of plant leaves.

By orienting our fabrication process around bulk procedures — actions that can be performed in one or more “sweeps”, such as casting, photo-etching, and laser cutting — we eliminate the many individual manufacturing steps that are common in more module-driven designs. These modular pneumatic surfaces consist of separate cells that are each tied to independent solenoid valves [11, 35]; in contrast, our approach allows for the creation of variable-sized arrays within a fixed number of fabrication steps.

This layer-driven design integrates well with the type of composite transducers that have taken hold within the soft robotics community [2], providing a scalable bed of actuators that can replace networks of individually connected tubes. Such a system may be well-suited for the production of room-scale pneumatic surfaces [59, 61], which, like current toolkits [22, 37, 53], have so far relied on a modular approach. Composite arrays such as *Stoma-Board*, which simplify manufacturing through the use of bulk-fabricated layers, may bring large-scale structures and high-resolution surfaces within reach.

2 LAYER-DRIVEN DESIGN

In Figure 2, we illustrate the driving principle of our design process: functionality arises from a stacked configuration of bulk-fabricated layers, rather than the assembly of many individual parts. (We observe that sufficiently mature robotic processes, such as “pick-and-place” or 3D-printing, may also be considered bulk procedures.) Though this imposes an additional engineering challenge during the development of the primary actuation mechanism, the resulting material cell will necessarily be scalable under this framework. Such designs are distinguished by four characteristics:

¹<https://en.wikipedia.org/wiki/BrailleNote>

- (1) *Constituent actuators are not distinct components, but instead cells within a common substrate.* In our implementation, this substrate is a patterned electrode array, with each node able to exert an attractive force on one section of a shared diaphragm.
- (2) *Communication, and in some cases computation, is not centralized, but instead distributed throughout the surface.* Neighboring cells exchange messages with each other, which our system exhibits by means of a daisy-chained control scheme.
- (3) *Energy is not delivered through individual connections, but instead made available through a globally accessible reservoir.* Analogous to the power and ground planes that have long been a staple of multi-layer circuit boards, the base layer of our system is a vacuum-connected cavity that acts as a global pneumatic sink.
- (4) *Pattern generation precedes fabrication and assembly.* In a module-driven design, actuators may be built independently, and then placed in positions across a surface. In our system, patterning must take place earlier in the design process, as all actuators are built concurrently during the layer-stacking assembly procedure. We implement a simple computational tool to generate these layouts.

We demonstrate the validity of this approach through the fabrication of a programmable surface, which serves as a "raw" base layer for mounting multiple types of pneumatic transducers.

3 BACKGROUND AND RELATED WORK

3.1 Shape-Changing Surfaces and Tactile Displays

Programmable surfaces can be broadly separated into two categories — dynamic matter (collections of actuators) that can be arbitrarily reconfigured [25, 32, 50, 69], and “morphing” materials, for which certain shape-changing capabilities are encoded as part of the fabrication process [12, 43, 64]. Our system is an instance of the former, but we leverage the composite material fabrication techniques that are common in the latter.

A popular instance of the first type of material is the “pin display” [27]. This is a two-dimensional surface, composed of linear actuators (pins) that can independently extend out-of-plane. Pins can be rigid, driven by miniature lead screw assemblies [54, 68], as well as soft, driven pneumatically [44]. This type of modular construction trades scalability for precise actuation — pins move independently, but the discrete assembly process imposes a practical limit on the number that can be fabricated.

Work by Zárate et al. [69, 70] hints at a solution. Their variant of a tactile display, while still consisting of individual (magnetic) pins, is driven by coils that are patterned on a printed circuit board. Since these multiple coils are all formed as part of a single fabrication step (photo-etching, during the printed circuit board manufacturing process), this act of patterning reduces the ultimate assembly time for the device. These copper traces can similarly be used for within-plane steering of magnetic markers [39, 58], and stand in contrast to prior approaches that employed beds of individually packaged solenoids [38, 65]. Notably, there is a trade-off here — while these layered coils can be replicated across large surfaces with relative ease, they are generally less powerful than their discrete counterparts (owing to the reduced number of turns).

One way to circumvent this dilemma is by using patterned elements as a means of “tapping in” to a larger energy source. Under this paradigm, power and control are fully decoupled, and the actuators serve as gateways to a global reservoir. Qiu et al. [42] employ this approach, spray-coating an array of resistive traces onto an electroactive polymer film, which is suspended above a pressurized pneumatic chamber. Through targeted Joule-heating of the film (via the resistive traces), they force heat-softened sections of the membrane to deflect outward and raise a layer of pins. Previously, Besse et al. [6, 7] demonstrated a similar design, fabricating a shape-memory polymer membrane with integrated heating elements. This membrane was mounted over an alternating pressure source — positive pressure pushes the selected areas upward, and negative pressure pulls them back down.

Our Stoma-Board system makes use of this "patterned gates" strategy as well, with an array of layered, miniature valves that connect an upper transducer layer to a pneumatic sink. In contrast to related approaches, which use an external bank of solenoid valves to inflate sections of a membrane [36, 49], our actuators are directly integrated into the surface, and do not need to be discretely assembled. Layered composites, then, may be key in creating programmable surfaces that can scale in size and density.

3.2 Soft and Foldable Robots

Roboticians, in recent years, have been drawn to composites as well — with some eschewing traditional linkages in favor of flat materials that fold or stretch [40, 47]. By stacking layers with dissimilar mechanical properties, or by cutting patterns into overlapping sheets [56], sections of the resultant material can be constrained to move along predefined paths when actuated. In a soft robot, for example, a bending motion might be achieved by depositing a compliant silicone layer on top of a more rigid, strain-resisting substrate. When subjected to an axial force, either via piezoelectric [66], electrostatic [5], or pneumatic actuation [29], the material curves in the direction of the less-stiff layer.

By micro-machining these individual layers (selectively removing material), bending behaviors can be further restricted to specific regions of the composite. This enables "pop-up" mechanisms, such as the origami-inspired joystick by Mintchev et al. [33], or the millimeter-scale delta robot by McClintock et al. [31]. In each of these systems, the composites consist of a flexible layer (polyimide), sandwiched between two rigid layers (fiberglass, or carbon-fiber). Strategic cuts in these layers give rise to Sarrus linkages, which lift sections of the composite out-of-plane. (These particular mechanisms are both driven by external base-stations, though other researchers have begun to explore foldable composites with self-actuating inner layers [60].)

Further embracing deformation, roboticists such as Kellaris et al. [20] achieve out-of-plane motion through the manipulation of flexible, fluid-filled membranes. These sandwich-style actuators are characterized by "zippering" motions — as portions of the outer membranes are squeezed together, an inner layer of fluid flows into a predefined pocket, causing the membranes to bulge outward. This squeezing is initiated by an applied electrostatic force, similar to the operation of dielectric elastomer actuators. Artificial muscles such as these can be fabricated from stacked thermoplastic sheets, which are then heat-sealed, filled with fluid, and patterned with compliant electrodes [34]. Other researchers have used similar constructions for the production of wearable haptic interfaces [28], indicating that this may be a viable technique for the creation of programmable surfaces.

For these devices, electrostatic actuation is a reasonable choice. It is a low-power method, only drawing current during transient periods; and at small distances, these actuators can provide a significant amount of force. We discuss this further in the next section.

3.3 Electrostatic Actuators

Two charged objects of opposite polarity, when placed in close enough proximity, will begin to move towards each other as they experience an attractive electrostatic force. This seemingly straightforward transformation of electrical energy into mechanical work has seeded a significant body of research relating to electrostatic actuators — perhaps most widely in the MEMS community. Here, investigators have leveraged this principle to develop micro-scale (sub-millimeter) sensors, switches, pumps, and valves [72]. Many of these devices incorporate some displacement mechanism, consisting of an anchored electrode that pushes or pulls a moveable plate.

At the meso-scale (centimeter) and larger, this attractive electrostatic force has been harnessed for braking and locking — modulating the frictional force between two electrodes that slide against one another. Diller et al. explored this through the construction of an electrostatic clutch, engaging and disengaging spring elements in a leg exoskeleton [9]. Hinchet et al. developed a similar concept, for grasping in virtual reality [14]. Their slimmer strips were worn on the fingers, constraining hand movement when a voltage was applied. Recent work

by Zhang et al. [71] has adapted this technique for use in for shape-changing pin displays — individual braking mechanisms will lock brass pins in place as a global upward force is applied, resulting in a reconfigurable height field.

An advantage of this friction-based mechanism is that during operation, the components are always in close proximity, where electrostatic forces are strongest. (These forces fall off with the square of the distance between charged elements.) Consequently, such systems have been able to bear human-scale forces (up to 100 N for the 10 cm wide electrode pairs in [9]). A key consideration is that the direction of actuation is normal to the applied electrostatic force (i.e. attraction up and down prevents sliding from left to right).

This has not typically been the case with regard to valves, for which electrostatic forces must resist an applied pressure directly. In the most basic construction [41], a flexible conductive diaphragm sits on top of an insulated electrode, covering a hole in the center of that electrode. When a voltage is applied, the attractive electrostatic force creates a seal over the hole, restricting air flow (Figure 6).

The difficulty here is that as soon as a small gap emerges, a peeling effect rapidly dislodges the diaphragm. As a result, valves with this construction are often constrained to operate within low pressure conditions (1 kPa) [8], or to be driven with high voltages (>600 V) [3].

To address this limitation, researchers have used additional pneumatic ports, which serve to balance the applied pressure and hold the diaphragm in place [4, 62, 67]. This, however, requires a second pneumatic source (one that sits just below the input pressure), which increases the overall fabrication complexity. In the next section, we introduce a novel valve design that overcomes this problem without the addition of extra pneumatic channels. By inverting the diaphragm actuation mechanism, such that it acts as a check valve rather than a lid or a cap, we are able to regulate pressures 80 times larger than comparable implementations [8] — a necessary performance increase for working with human-scale forces.

4 PATTERNED VALVES FOR PROGRAMMABLE SURFACES

In the remainder of this paper, we describe the design and fabrication of a material that emerges from our layer-driven framework: *Stoma-Board*. This is an array of patterned, electrostatic valves, situated on top of a global cavity (Figure 3a, 3b). By switching individual valves on and off, we are able to control the flow of air into a transducer layer on top of the board. For instance, as shown in Figure 3d, we can regulate airflow into discrete pockets of an elastic substrate (causing these cells to inflate, buckle, or bend, depending on the geometry).

Many programmable surfaces, if they are discretely actuated, more often resemble collections of machines than they do continuous matter. This is due in part to the limitations of a module-driven design — if actuators are assembled as independent components, increased resolution comes at a high manufacturing cost. Our aim at the outset of this work was to solve this by identifying a fabrication process for which assembly time is proportional to the number of layers, rather than the number of actuators. This decoupling allows us to pack more actuators into the same area with little or no additional time loss.

Researchers in MEMS have long embraced lithography as a means of achieving this type of feature density [63]. However, industrial processes in the this area are usually optimized for the production of singular devices at the micro-scale (accelerometers, gyroscopes, etc.), as opposed to networks of actuators that extend over a centimeter-scale surface area or larger. For this more expansive application, we looked towards the already-mature process of printed circuit board (PCB) manufacturing, and focused on integration into that pipeline.

PCB manufacturing is characterized by patterning, etching, and layup (stacking and bonding layers) [16]. Most fabricators start with a copper-clad fiberglass sheet, and begin production by applying a photosensitive coating and printed mask. They follow these steps with a chemical procedure that selectively removes exposed copper from the substrate. For boards with more than two layers, additional material is then stacked around the core and laminated together — usually with an insulating dielectric on both sides of the sheet, and copper foil on the outer

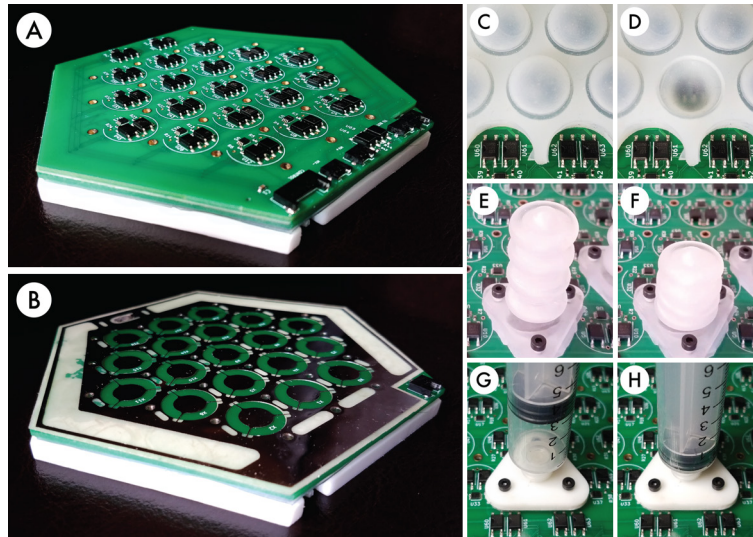


Fig. 3. One of our 19-cell Stoma-Boards (a). Directly below the top circuit board is a conductive diaphragm (b), which regulates air flow into a global reservoir. Cells are individually addressable. We treat Stoma-Board as a "raw material", using it with different transducer layers to build a variety of devices. Example transducers include: (c,d) Bistable dome, part of a larger cast membrane. (e,f) 3D-printed bellows-style transducer, which contracts under negative pressure. (g,h) Rigid Luer-lock attachment, connected to a syringe for linear actuation.

layers. This new material can be etched again, and the process may be repeated as more layers are added (such that a multi-layer board is effectively a sandwich of smaller sub-boards). Some complex PCBs, particularly those with embedded electronic components, are actually composites of other fully drilled, plated, and soldered circuit boards [55].

From this standpoint, the Stoma-Board layers that we introduce can be seen as an extension of this manufacturing process – a few extra steps during the layout and bonding stage. The result of our procedure is a composite material with integrated electronic and pneumatic components (Figure 4). From top to bottom, these layers are:

- (1) An application-dependent transducer. (For example, an elastic surface, with air-filled pockets that buckle or bend when actuated.)
- (2) A printed circuit board, with control circuitry on top, and patterned electrodes on the underside.
- (3) A metallized polyester diaphragm (Mylar, 25 μm), which regulates air flow.
- (4) A natural rubber spacer (150 μm), through which the diaphragm travels.
- (5) A second printed circuit board, with patterned electrodes on top.
- (6) An SLA 3D-printed cavity, which serves as a global pneumatic sink.

Note that although each layer is manufactured by a bulk process (casting, etching, laser-cutting, or machine placement), we still retain the ability to dynamically actuate discrete subsections of the finished surface.

4.1 Working Principle

Air flow through each valve is regulated by a metallized polyester diaphragm, which rests underneath an insulated copper electrode (Figure 4). This diaphragm cell is connected to the greater membrane layer by three hinges (Figure 4i), which allow it to flex out of plane.

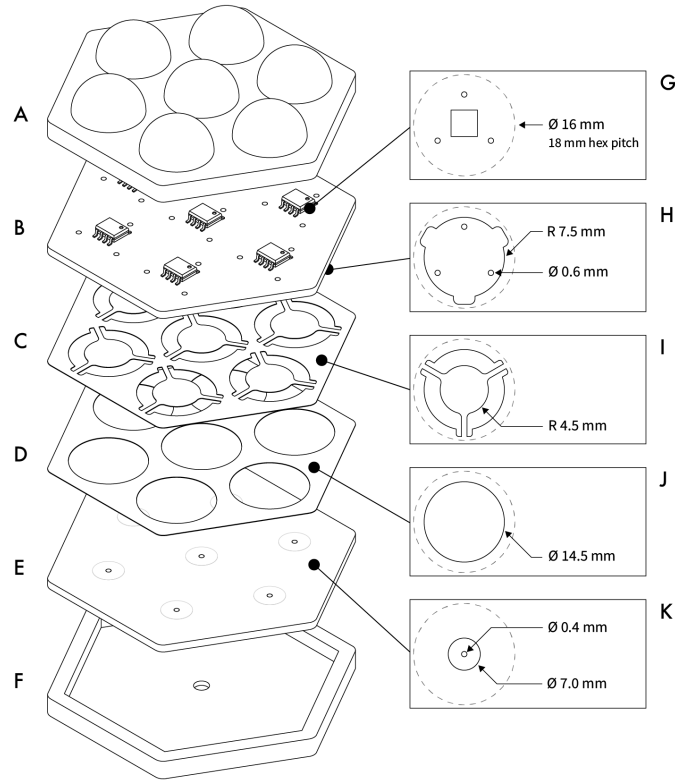


Fig. 4. Exploded view of the Stoma-Board structure. The transducer layer (a), in this case, is an elastic surface, composed of multiple pockets that can inflate, buckle, or bend independently. Air flow into this layer is regulated by a flexible, conductive diaphragm (c, i). When a vacuum is applied, this diaphragm deflects downward through a rubber spacer layer (d, j), and is pulled flat against an outlet (e, k). This closes the valve and (in this example) traps air inside the pockets of (a). To open the valve and allow air to flow, an electric charge is applied to an electrode (h) on the underside of a printed circuit board (b). Electrostatic forces retract the diaphragm from the valve outlet, allowing air to move from the transducer layer (a) to a global sink (f). Cells are hexagonally packed, with an 18mm pitch.

In the active state (when a voltage is applied), electrostatic forces hold the diaphragm in place, and air passes freely from inlet to outlet (Figure 5a). In the non-active state, negative pressure at the valve outlet instead pulls the diaphragm downstream, blocking the outlet and impeding further flow (Figure 5b). To mitigate leakage in the non-active state, an optional secondary electrode at the outlet can be activated and used to further seal the valve (Figure 5c). Throughout this paper, we will refer to the first electrode as the valve-opening electrode, and the second electrode as the valve-sealing electrode.

The attractive force between (either) electrode and the valve diaphragm is expressed by the relationship:

$$F \propto \frac{V^2 A}{d^2}$$

where F is the electrostatic force, A is the overlapping electrode area, V is the applied voltage, and d is the distance

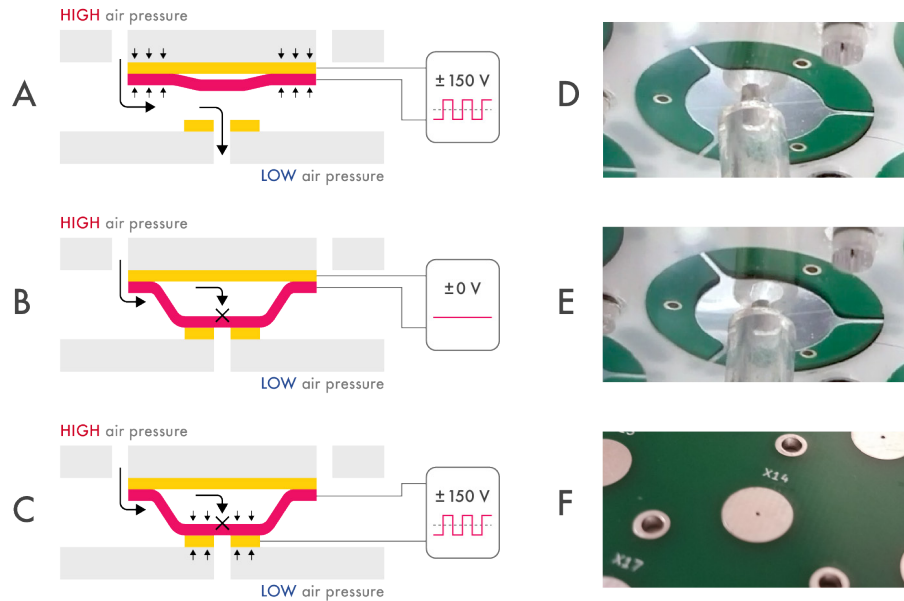


Fig. 5. The three states of operation. (a) *Active state*: A voltage is applied between the valve-opening electrode and the conductive diaphragm. The resulting electrostatic force causes the diaphragm to adhere to this electrode, allowing air to pass underneath. (b) *Non-active state*: If no voltage is applied, a pressure differential will pull the diaphragm flat against the valve outlet, restricting air flow. (c) *Sealed state*: A voltage is applied between the conductive diaphragm and the valve-sealing electrode. Electrostatic forces pull the diaphragm tight against the outlet, mitigating leakage. (d,e) Diaphragm and valve-opening electrode in active (open) and non-active (blocking flow) states. To show actuation in these photographs, a clear acrylic plate is used in place of the opaque valve-sealing electrode. (f) An image of the valve-sealing electrode, by itself.

between the electrode and the diaphragm [3]. For an electrostatic valve, the parameter of greatest concern is the distance d (the other two right-side variables can be readily controlled, but this distance will vary during operation). Since the attractive force decreases with the square of this value, small fluctuations in distance have large consequences for valve behavior.

In particular, electrostatic latching mechanisms such as these are often susceptible to “peeling” [18]; and some valve geometries are more vulnerable than others. One of these configurations is shown in Figure 6, in which the diaphragm is positioned to block incoming flow from below, as opposed to sealing outgoing leakage from above. As soon as a minor gap emerges under the diaphragm (due to pressure fluctuations, surface roughness, or other environmental factors), the electrostatic force at that interface is greatly diminished. This reduction in force means that a section of the diaphragm may begin to balloon or lift away, propagating until the seal is fully broken. Our earliest prototypes were built in this style, and (just as in similar implementations [8]), they were unable to regulate pressures above several kilopascals.

It is possible to address this limitation by adding additional pneumatic sources and channels, in order to keep the pressure differential around the diaphragm within a small threshold [4, 62, 67]. But seeking a simpler construction, we took an alternate approach – by inverting the diaphragm configuration as described earlier (Figure 5a-c), we were able to take advantage of a “zippering” effect [52] to actuate the valve.

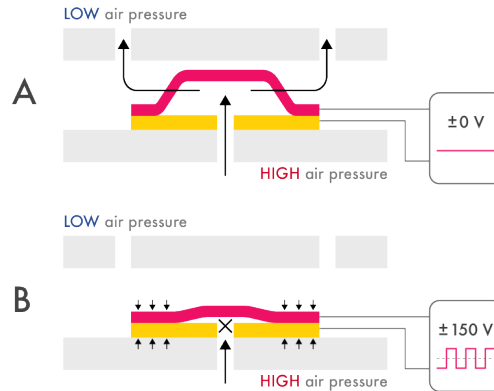


Fig. 6. Early Stoma-Board prototypes used an alternate valve configuration, inspired by common MEMS implementations [41]. The diaphragm rests above the valve inlet, and when actuated, blocks air flow from below (b). At pressures beyond 1 kPa, small gaps begin to emerge at the valve inlet, which propagate across the surface and eventually dislodge the diaphragm [8]. When no voltage is applied, air passes through the valve unimpeded (a).

“Zippering” motions, in our system, start at the hinges of the diaphragm and move inward. Consider the valve in the non-active state (Figure 5b): negative pressure has pulled the diaphragm flat against the outlet. This is $150\ \mu\text{m}$ below the valve-opening electrode — small on a human scale, but large enough for electrostatic forces to be noticeably weakened. The diaphragm hinges, by contrast, are ten times closer — separated only by a thin dielectric layer, just $15\ \mu\text{m}$ thick. When we switch to the active state, strong electrostatic forces near the hinges allow us to retract a diaphragm that would otherwise be out of reach at high negative pressures ($> 80\ \text{kPa}$).

4.2 Insulating Dielectric and Driving Voltage

When we apply a voltage between an electrode and the valve diaphragm, an insulating layer is needed in the middle to prevent electrical shorts. In early prototypes, we used $25\ \mu\text{m}$ polyimide sheets, hand-laminated onto bare copper electrodes. (This technique is similar to [14], though we did not use any adhesive.) Polyimide is a natural choice for this layer — with a breakdown voltage in excess of $250\ \text{V}/\mu\text{m}$, we can administer several kilovolts before the insulating layer fails and conducts.

Our system, however, operates between 150V and 300V (drawing a low and safe $50\ \mu\text{A}$). At these levels, a thin layer of solder mask (breakdown voltage around $25\text{--}30\ \text{V}/\mu\text{m}$) is sufficient insulation, with the additional benefit of a smaller minimum distance d between conductors. Consequently, we use only solder mask to separate the valve-opening electrode from the metallized side of the diaphragm.

The valve-sealing electrode is left exposed (bare copper). It does not contact the metallized side of the diaphragm — the $25\ \mu\text{m}$ Mylar sheet itself provides adequate insulation.

4.3 Daisy-Chain Electronic Communication

Fully distributed computation is a target that arises from the layer-driven model (and is addressed briefly in Section 7). This is desirable not only from a fabrication perspective (eliminating multiple physical connections to a central hub), but also important for making robust programmable materials that scale without regard to the processing power of a master controller.

A first step towards this objective is casting each material subsection as a distinct computational node, capable of communication with its immediate neighbors. We implement this (somewhat simply) in our system by means of a daisy-chained control scheme.

Physically, this communication takes place in the layer above the valve diaphragm (Figure 4b). Each material cell contains several discrete electronic components, as well as the patterned copper circuitry that connects them, which includes the valve-opening electrode. A shared clock line and global power sources (high-voltage rails for actuation and low-voltage rails for signaling) run across the surface and are accessible by each cell.

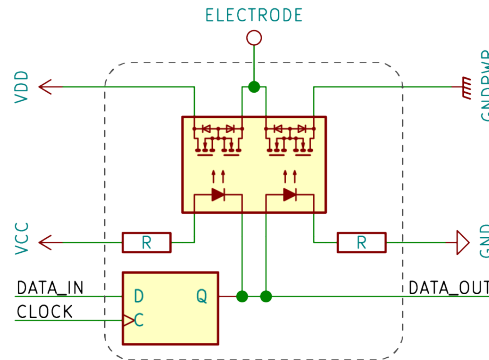


Fig. 7. Electronic components within a Stoma-Board cell. Cells are daisy-chained, and change state in response to a global clock signal.

A simplified schematic is shown in Figure 7. An electrode may be connected to either of the high voltage rails through a pair of opto-isolated solid-state relays². A discrete flip-flop³ drives the LEDs of the opto-isolator, and also serves as the main communication element. On every clock pulse, the cell as a whole follows two rules:

- (1) Pass the current cell state to the right-side neighbor.
- (2) Receive a new cell state from the left-side neighbor.

With this configuration, an external microcontroller upstream can quickly send data to all nodes in the chain. This operation is similar to that of the addressable LED strings (such as the APA102 or WS2812) that in recent years have served a material-like role in maker and DIY communities [30]. Our clock signal runs at 300 kHz, which allows us to set the state of 300 valves per millisecond. This rapid switching means that in practice, the overall refresh rate of the surface is generally independent from the number of valves, and instead a function of the pneumatic control scheme (see Section 4.4).

Opto-isolated relays are not the only driver option. In earlier prototypes, we used resistor-transistor logic to control the valve array – electrodes were either actively switched low or passively pulled high. Though smaller in footprint, which is desirable, this design wastes power on the actuation side, continuously sending current through the resistor when the electrode is held low. A more efficient half-bridge topology was also considered, but ultimately discarded due to the need for additional high-voltage bias supplies. While the package size of the solid-state relays did limit our electrode density, we decided that the reduced complexity, low-power actuation, and isolation benefits made them a reasonable choice for this implementation.

²Cosmo Electronics KAQY214S

³Texas Instruments SN74LCV1G74

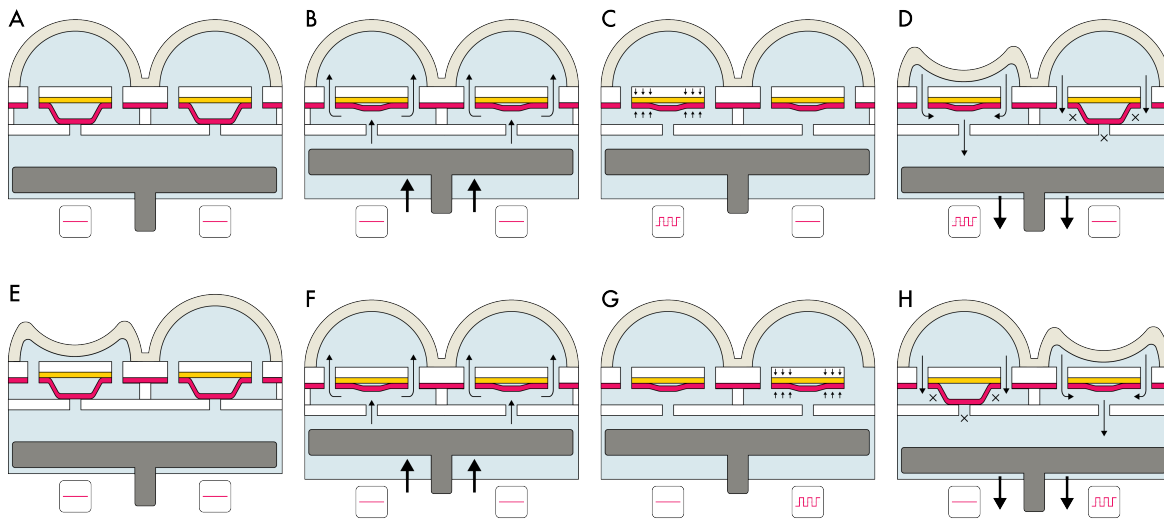


Fig. 8. The "push-pull" actuation sequence for driving Stoma-Board prototypes using bi-stable silicone domes. (The alternating pressure source is represented by a moving piston, in gray.) Initially, the system is at rest (a). When positive pressure is created in the global reservoir, all diaphragm cells are pushed upward towards the top electrodes (b). At this stage, we may apply a voltage to latch one or more diaphragm cells in place (c, left). When negative pressure is created in the global reservoir, air exits the latched cells, and the elastic structures buckle (d, left). Note that in the unlatched cells, the elastic structures remains upright, as the diaphragm prevents air from escaping (d, right). If we remove the applied voltage, the valves may close, but the buckled cells remain unchanged (e, left). To restore these cells, we can again create a positive pressure (f), at which point we may choose to actuate another group of cells by the same process (f-h). The global pressure oscillations effectively determine the "refresh rate" of the Stoma-Board.

4.4 Pneumatic Push-Pull Control Scheme

The bottom layer of our Stoma-Board (Figure 4f) is a global reservoir, which typically acts as a pneumatic sink (negative pressure, pulling air down through the material). The presence of this common driver has implications for the design of the transducer layer, as well as for the actuation control scheme.

Consider the following example, relating to the silicone domes in Figure 3c. An open valve allows air to flow from a pocket in the top layer to the global sink, deflating or depressurizing that top pocket in the process. Closing the valve will restrict that air flow, preventing further deflation – but this stoppage alone can not put the top pocket back in the inflated or neutral position.

In order for this layer to "rebound", spring forces in the elastomer must overcome the negative air pressure within the cell. One way to address this is by strategically adding drain holes in the top layer, allowing outside air to leak into the cell so that the pressure can begin to equalize. However, for more predictable behavior, we can instead use the "push-pull" actuation scheme outlined in Figure 8. Under this scheme, a global reservoir is connected to an alternating pressure source (such as the syringe pump in Figure 9). During the "pull" stroke, air flows out of the Stoma-Board, and actuated cells buckle under the negative pressure. During the "push" stroke, positive pressure restores all cells to their upright positions.

For this procedure, the global reservoir is connected to a variable source, which alternates between positive and negative pressure. To generate this behavior, we use a custom syringe pump (Figure 9). In the "push" stage,



Fig. 9. The linear-actuator syringe pump used to pneumatically drive our Stoma-Board surfaces.

air is forced upward through the valves, into every cell of the top layer. In the “pull” stage, air is drawn out of the system — but only through valves that are in the active state.

Note that since every cell is affected by the “push” stroke, the transducer layer is fully inflated between refreshes. For some applications, such as refreshable Braille displays, this is sufficient [48]. However, if more dynamic control is desired, then a secondary valve layer is necessary to block the positive pressure from the “push” stroke. (We describe such a construction in Section 8.4.)

While we use a syringe pump in our applications, any alternating pneumatic source will suffice. Ultimately, it is the frequency of this source that determines the refresh rate of a Stoma-Board surface. If fast refreshes are necessary, then the flow rate of the pump must large enough to quickly pressurize and depressurize the global cavity.

5 FABRICATION PROCESS

5.1 Cutting: Diaphragm and Spacer

The Stoma-Board diaphragm is laser-cut from a 25 μm thick Mylar film, metallized on one side (CS Hyde 48-1F-1M). It is important that this film is held flat during the cutting process — if manufactured imprecisely, it may kink or buckle out-of-plane when aligned with the electrode array. We solve this by first laminating the uncut Mylar film onto a sacrificial acrylic sheet (using isopropyl alcohol and a rubber squeegee), which lies flat on the laser bed. After the cut, we peel the finished diaphragm off of the acrylic substrate in a single step, with no weeding or deburring necessary.

Notice that our diaphragm is cut with a small tab near the bottom edge (Figure 10c). Later, in the layup process, we use silver epoxy (MG Chemicals 8331) to adhere this tab to an exposed copper pad on our circuit board.

The spacer (Figure 4d) that separates the diaphragm from the valve outlet is cut from a sheet of natural gum rubber, 150 μm thick (McMaster-Carr 8611K11). The fabrication process is similar to the one described above — the rubber is laid flat on an acrylic sheet prior to the cut, and peeled away afterwards in a single motion. We first experimented with rigid spacers (polyester sheets ranging from 50 to 250 μm), but ultimately found that a more compliant material led to better valve performance, perhaps due to a tighter pneumatic seal.

For some prototypes, we used this same rubber material as a bottom gasket layer, which sits between the valve-sealing electrodes (Figure 4e) and the common cavity or printed piping structure (Figure 4f). These gaskets were cut in the same manner as the spacer.

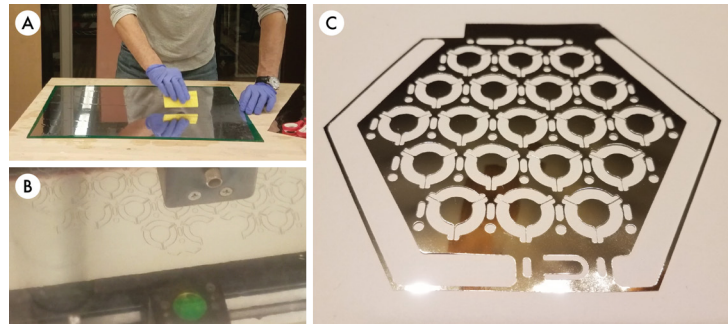


Fig. 10. To fabricate the diaphragm, we first use isopropyl alcohol and a rubber squeegee to laminate a metallized Mylar film onto an acrylic sheet (a). The diaphragm pattern is then laser cut (b), and the finished diaphragm is removed (c).

5.2 Casting: Upper Gasket and Soft Transducers

For the top layer of our system, we tested a variety of custom-made transducers. Some of these were 3D-printed (Formlabs Elastic Resin 50A), and some of them were cast (Smooth-On Dragon Skin 30 and Mold Star 30). Additionally, some experiments required a rigid manifold, which sat on top of a cast gasket layer.

To begin the casting process, we first spray a release agent (Mann Ease Release 200) onto a two-piece 3D-printed mold (Figure 11). This mold is left to sit for ten minutes. In that interval, the uncured silicone is mixed and degassed at -27 inHg, in order to remove any large air pockets. The silicone is then poured into the mold, and left to cure at room temperature for 16 hours.



Fig. 11. A 3D-printed mold used to cast one of our soft transducer layers (the bistable dome array).

5.3 Printing: Global Reservoir and Upper Manifold

Our Stoma-Board valves rest on common reservoir, used as a global pneumatic sink (Figure 12). While this could be a single, open cavity (CNC-milled, for example), we chose to 3D-print a connected pipe structure, in order to minimize the reservoir volume and allow for quicker pressure changes.

We also printed rigid manifold layers (Figure 19a) for mounting some of our elastic transducers. While these transducers could be fixed to the upper PCB directly, we found that the manifold helped to ease prototyping, as transducers of different geometries could be more easily swapped and tested.

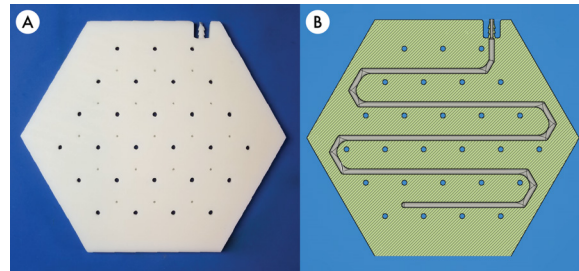


Fig. 12. (a) 3D-printed reservoir that serves as a global pneumatic sink. (b) Cross section.

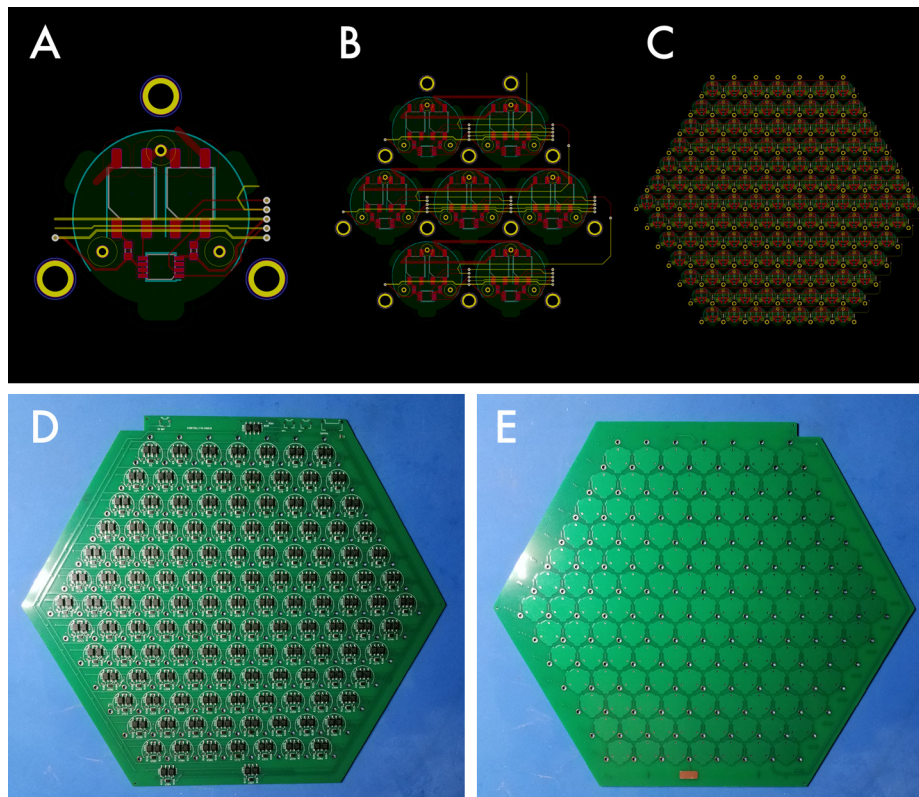


Fig. 13. Our command-line interface auto-generates KiCad-compatible design files, for hexagonal Stoma-Board patterns at multiple scales. (a) A single cell, with valve-opening electrode in green, pads for surface-mount components in red, valve inlets in yellow (small), and transducer mounting holes in yellow (large). (b,c) Patterns of 7 and 127 cells. (d,e) Fabricated circuit board, with electronic components on top (d) and patterned electrodes on bottom (e). Note that while our design software can produce Stoma-Board patterns at various scales, all actuation characteristics are measured from a 19-valve test rig, not the 127-valve board.

6 ACTUATION CHARACTERISTICS

There are two ways we might wish to actuate a cell of our Stoma-Board. We can either start with the global vacuum active and try to *lift* the valve diaphragm upwards; or we can first *latch* the valve diaphragm in the raised state, and apply a vacuum only after the valve is already open.

We make the distinction because Stoma-Board valves exhibit a degree of hysteresis (Figure 14). Once the diaphragm has been pulled close to the valve-opening electrode, the newly strengthened electrostatic forces tend to hold it in place, even if the voltage drops. (Recall that the electrostatic force between two objects is inversely proportional to the squared distance.)

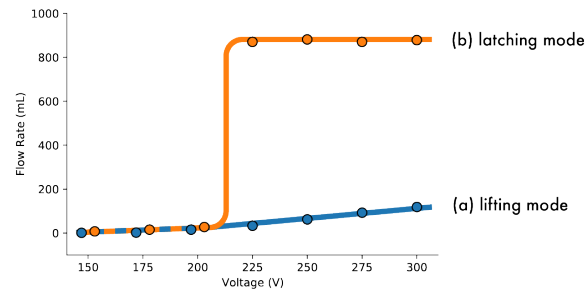


Fig. 14. Average flow rate through a single Stoma-Board valve ($\Delta P = 30$ kPa, $n = 3$) over a range of applied voltages. The behavior differs in lifting (vacuum-first) and latching (voltage-first) modes. (a) Lifting: Below 200V, negative pressure dominates this interaction and keeps the valve diaphragm closed. Beyond this point, air flow grows linearly as electrostatic forces lift the diaphragm away from the valve outlet. (b) Latching: If a valve is latched open before negative pressure is applied, electrostatic forces are stronger due to the reduced diaphragm distance. Above 200V, the valve remains fully open. Below this value, the diaphragm is pulled away from the valve-opening electrode, and behavior is similar to the lifting mode.

While the lifting mode is arguably more dynamic, the latching mode allows us drive the board at lower voltages, and circumvents some of the dielectric charging issues that we discuss in Section 7. This is also the mode used in our push-pull control scheme (Figure 8). However, for completeness, we report the actuation characteristics for both lifting and latching modes.

To facilitate our measurements, we attached a rigid manifold to the top of a 19-cell Stoma-Board (in place of the transducer layer). With Luer lock fittings for each cell, we were able to quickly add and remove mass flow sensors for evaluating actuator performance (Figure 15).

6.1 Opening Voltage

The opening voltage is associated with the lifting mode – it is the point at which electrostatic forces upward surpass pneumatic forces downward, and air begins to pass through the cell.

To measure the opening voltage for a given valve, we first applied a global negative pressure, which pulled the valve diaphragm closed. We then increased the voltage between the diaphragm and valve-opening electrode, in increments of 10V, until the diaphragm was attracted upwards and significant air flow through the valve was observed (25 mL/min).

Figure 16a charts the Stoma-Board opening voltage as a function of pressure (the differential between valve inlets and the global reservoir). At higher pressures (80 kPa), this approaches 300V, which we chose as the limit of our system. Beyond this point, we noticed an increase in parasitic effects.

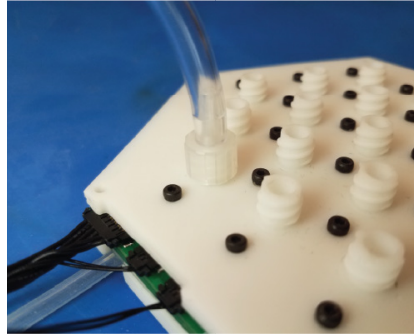


Fig. 15. Test rig for measuring the flow characteristics of a 19-cell Stoma-Board. A 3D-printed manifold with Luer-lock fittings allows for individual connections to flow sensors. A vacuum pump acts as a global negative pressure source, which can be manually adjusted with a breaker valve. Valve inlets are left at atmospheric pressure.

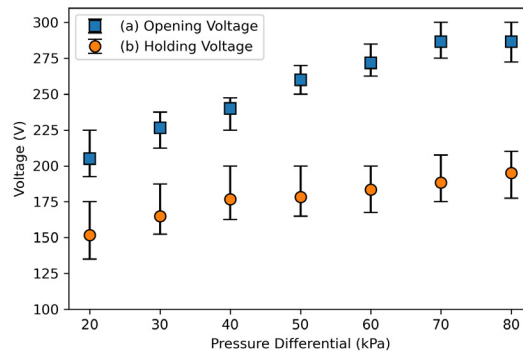


Fig. 16. Average opening voltage (lifting mode) and holding voltage (latching mode) across a range of pressure differentials. Valves were sampled uniformly from the 19-cell test rig in Figure 15. Error bars represent 25th and 75th percentiles ($n=7$).

Though the valves in our application examples all occupy discrete “on” and “off” states, we can achieve variable flow rates (between “fully on” and “fully off”) by driving the system at higher or lower voltages respectively. Figure 17 shows this relationship for six valves at several operating pressures (sampled randomly from our test rig). Below 150 to 200 volts, the applied vacuum dominates this interaction. As the voltage increases beyond this point, air flow through the valve increases as electrostatic forces lift the diaphragm away from the valve outlet. We did not observe any pneumatic crosstalk during these tests – flow rates through neighboring valves stood unchanged.

Stoma-Board cells remain robust throughout repeated actuations. In Figure 18, we plot the average opening times for an additional six valves, over the course of one hundred trials. Operating at 300 volts, and subject to 80 kPa, the average valve opens in less than 40 milliseconds. Notice that there is no degradation over repeated trials – the average opening time for the final 25 actuations (36 ms) is comparable to the average opening time for the first 25 actuations (38 ms). We discuss reliability further in Section 8.

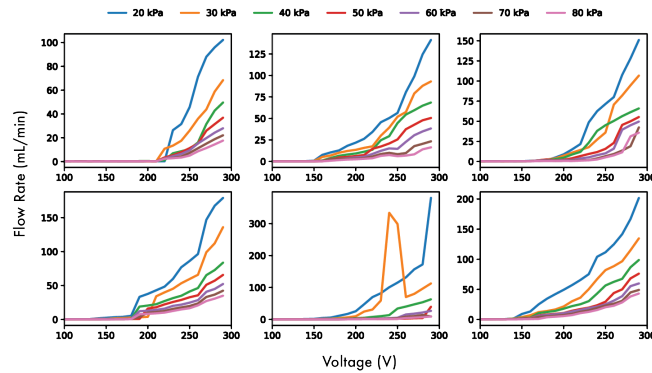


Fig. 17. Flow rates for six randomly sampled Stoma-Board valves, as a function of opening voltage. Note that for one valve (middle, bottom) there was a flow rate spike at 30 kPa and 240 V. This anomaly did not reoccur during a second test of the same valve, but we include it here for transparency.

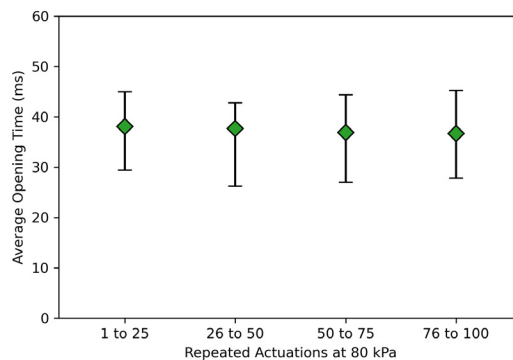


Fig. 18. Average opening times for six randomly sampled Stoma-Board valves, over 100 trials. (Opening times are averaged on a per-valve basis, and then these values are averaged to produce the green data points.) Note that opening times remain consistent throughout the experiment. Operating conditions: 80 kPa, 300 V. Error bars represent 25th and 75th percentiles.

6.2 Holding Voltage

Since our applications use an alternating pressure source, we are able to take advantage of the latching mode, and activate valves before a negative pressure is applied. In this context, the quantity of interest is the holding voltage – the minimum voltage required to keep the valve from closing (once the pressure in the global reservoir drops). This value is smaller than the opening voltage, due to the reduced distance between the diaphragm and the valve-opening electrode in the initial state.

To measure the holding voltage (Figure 16b), we first applied 300 volts to the valve of interest. We then applied a negative pressure, and recorded the steady-state flow rate. Finally, we progressively lowered the valve voltage (in increments of 10 volts), until the flow rate dropped below ten percent of the steady-state value. This drop-off does not happen gradually – as show in Figure 14, there is a "cliff" at which point the valve transitions from fully-open to nearly-closed.

7 PROGRAMMABLE STOMA-BOARD SURFACES

From a stock piece of wood or plastic, a craftsperson can construct a multitude of objects, each with mechanical properties that are (in part) a function of the original workpiece. Porous sheets of fiberboard, for instance, can be shaped into a vacuum table; and compliant strips of bamboo can be woven into a flexible basket. Similarly, we envision a process in which a fabricator may start with a sheet of “raw” Stoma-Board, and through the addition of custom transducers, arrive at a variety of programmable surfaces and mechanisms. Importantly, the scalable production of this base material (i.e. patterned valves) is only made possible by the layer-driven manufacturing techniques that we employ.

In this section, we showcase four surfaces (using three types of transducers) that are built upon our “raw” Stoma-Board surface.

7.1 Tactile Patterns from a Bistable Membrane

7.1.1 Standard Pitch. Bistable mechanisms do not require an external energy source in order to maintain their state, which makes them an attractive transducer option in low-power applications [46]. For our first demo, we cast an elastic silicone membrane (Smooth-On Dragon Skin 30), composed of bistable, hemispherical cells (Figure 19). While it’s possible to attach to this membrane to the raw Stoma-Board directly, we opted to use a 3D-printed manifold as an intermediate layer for ease of mounting.

Initially, all cells are in the raised state. To render a tactile pattern, we latch open the relevant valves, and apply a global negative pressure — this causes the selected cells to buckle into the collapsed state. To return the cells to the raised state, we apply a global positive pressure.

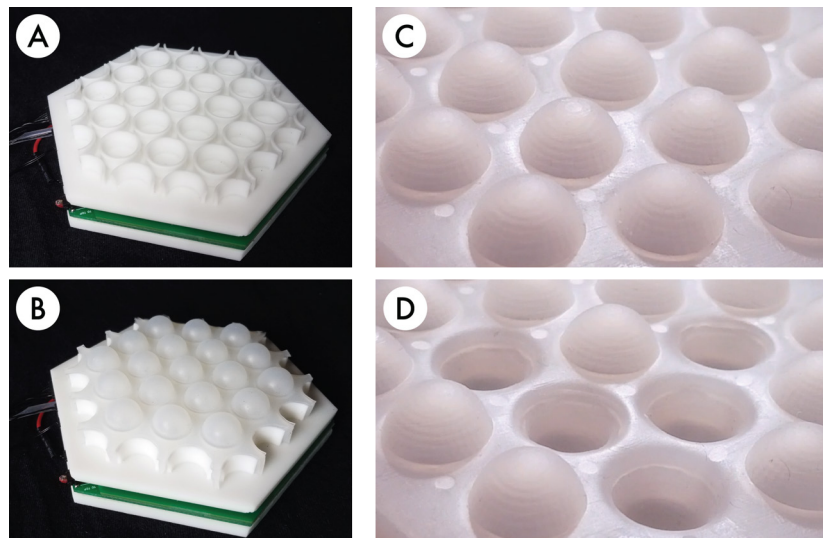


Fig. 19. We mount a cast array of bistable domes (b) on a 3D-printed manifold (a). By activating specific valves, we can render tactile patterns (c,d). Domes are 14 mm in diameter.

7.1.2 Compact Pitch. By altering the channel structure of the upper manifold, we can modify the apparent density of the Stoma-Board surface. In our second demo (Figure 20), a set of converging pipes decreases the cell pitch to 2.5 mm (Braille spacing), such that six transducers can fit within the area of a human fingertip. At this scale, the raised domes are more readily perceived as a texture, as opposed to a group of distinguishable objects

[26]. While the perimeter of the Stoma-Board is still determined by the electrode and membrane layers, this flexibility in piping can hasten the prototyping of fine-grained (and variable-pitch) tactile interactions.

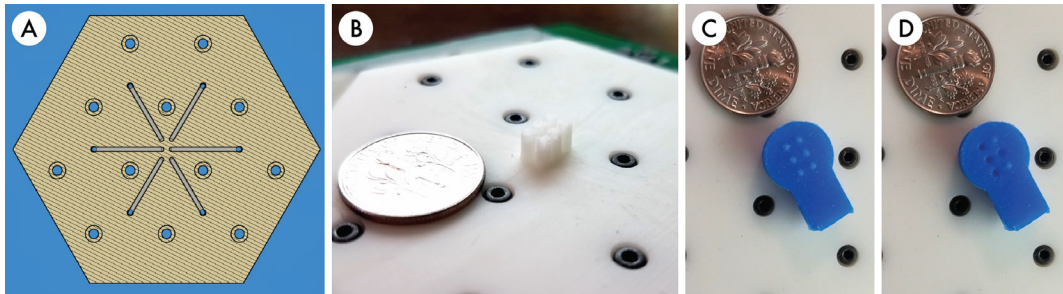


Fig. 20. A set of converging pipes, as seen in the manifold cross-section (a), shrink the transducer pitch to 2.5 mm (b). The Braille transducer (c,d) is cast silicone (Smooth-On Mold Star 30), and individual dots can be lowered when the corresponding Stoma-Board valves are opened.

7.2 Bellows-Style Robotic Actuators

Among soft roboticists, the bellows-style actuator (Figure 3e, 3f) is well-established as a means of converting pneumatic energy into linear motion [10]. When pressurized, it expands along a single axis. When de-pressurized, it contracts. If two or more are connected in parallel, an applied pressure differential will result in a bending motion, which forms the basis for many soft robotic joints [17].

Pneumatic routing is often a challenge when integrating these types of soft actuators. Since every bellows structure needs to be pressurized independently, many research prototypes rely on bundles of tubes, which tether the individual actuators to an external bank of valves.

With Stoma-Board as a base material, these valves can instead be embedded in the robot structure directly. In our third demo (Figure 21), three bellows-style transducers (SLA 3D-printed with Formlabs Elastic Resin 50A) are fixed to a raw Stoma-Board and used to drive a 2-DOF joint. By selectively opening valves and contracting individual transducers, we can determine the roll and pitch of an attached platform. These embedded valves may enable modular stacking, in a manner similar to the continuum robots by Robertson and Paik [45].

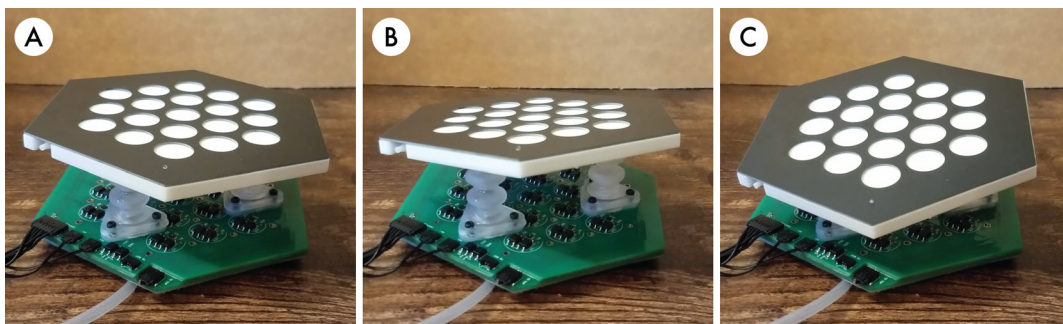


Fig. 21. 3D-printed bellows-style actuators control the orientation of an attached platform.

7.3 Spoke-Propelled Rimless Wheel

The "rimless wheel" is a rudimentary legged robot, suitable for traversing rough and uneven terrain [19]. In a typical implementation, the spokes of the wheel are passive elements, and a hub-mounted motor is used to drive the structure forward or backward [51]. To enable additional modes of locomotion, variants of this design have incorporated spokes that are independently actuated, which propel the robot by extending and contracting on command [15, 24]. This modification eliminates the heavy, motorized hub, but requires a separate mechanism for each leg of the robot. Building such an assembly can be cumbersome.

With a raw base of patterned valves, constructing this prototype becomes as simple as adding a custom transducer layer. In our fourth demo, we showcase a spoke-propelled rimless wheel (Figure 22), which can "walk" forward via a sequential extension of pneumatically-actuated legs. Note that in this example, the transducer layer and common cavity are swapped – we use a global pressure *source* instead of a pressure sink.

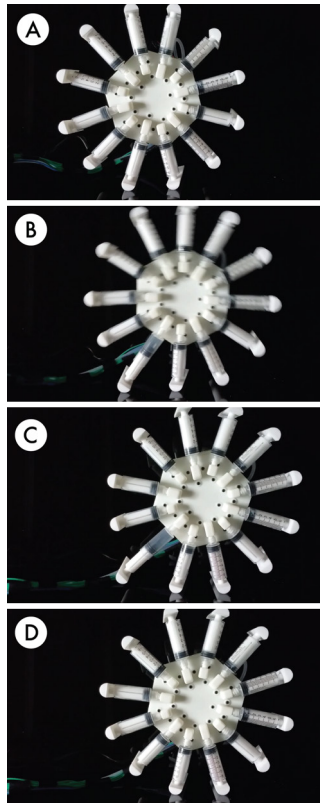


Fig. 22. An actuated rimless wheel, with spokes (syringes) that can extend independently. The syringe manifold is attached to a hexagonal Stoma-Board, which is connected to a single pressure source. In the stable position (a), two spokes maintain contact with the ground. When the left spoke is extended (by opening the appropriate Stoma-Board valve) the wheel tilts to the right (b). The wheel falls to a new stable position (c), and the extended spoke is retracted (d).

8 DISCUSSION, LIMITATIONS, AND FUTURE WORK

8.1 Long-Term Use

From a distance, electrostatic actuation appears deceptively simple — a straightforward mapping of an applied voltage to a resultant force. In reality, there are parasitic effects which can reduce the long-term reliability of such systems. The most significant of these, well-recognized by the MEMS community, is dielectric charging [23]. This is a molecular-scale phenomenon, which results from a displacement of polarized components within the material. If unaccounted for, this can lead to “sticky” switches (or in this context, valves).

In our Stoma-Board actuators, the dielectric layer is a thin coating of solder mask, which separates the conductive diaphragm from the valve-opening electrode. If a permanent charge develops in this dielectric layer, the diaphragm will always cling to the solder mask, and the valve will be unable to close. This parasitic charging often occurs after an extended period of exposure to a constant, applied voltage [14].

We were able to mitigate this effect by driving our actuators with a bipolar square wave (as opposed to a DC source), and reducing the peak voltage (no higher than 300 V). While this balancing of polarity over time was sufficient for our applications, it is possible that such adjustments may only reduce or delay this effect. Further reliability testing is needed in order to assess valve performance beyond the 100 trials described in Section 6.1.

8.2 Towards Larger Surfaces

A second concern relates to pneumatic actuation, and arises when working with large transducer membranes. Since these membranes are cast from 3D-printed molds, the printer’s working area determines the maximum size of a cast membrane. Larger membranes can be assembled from these smaller sections, but discontinuities at the section boundaries can lead to air leakage, and unpredictable actuation behavior. Future revisions may benefit from a less-dense actuator packing (allowing for a thicker, more robust section boundary) or flexures between cells to mitigate PCB bowing (which can become significant at larger scales, such as our 127 valve array).

In addition, the global cavity, instead of being 3D-printed, could itself be fabricated via a layer-driven approach. (Indeed, commercial manifolds⁴ exist that utilize this technique.) Stacking and bonding milled sheets may scale more easily than a purely additive procedure.

8.3 Towards Denser Surfaces

The electronic components that we use — in particular, the opto-isolated solid state relays — determine the minimum pitch of the raw Stoma-Board surface (18 mm). It is worth noting that these particular components are overpowered for our application, capable of switching currents that are orders of magnitude larger than necessary. With more refined electrical engineering, it is conceivable that this pitch could be reduced. However, as the size of the electrostatic actuators decrease, so too does the force. The tradeoffs in this area should be evaluated.

8.4 Bidirectional Valves

As noted in Section 4.4, valves in our system are designed to withstand pressure in only one direction. For many applications, such as those demonstrated in Section 7, this is sufficient. However, if bidirectional switching is necessary, a variation of this construction can be used. By adding an additional membrane (Figure 23), effectively placing two flap valves “back-to-back”, we can block (and switch) pressure in both directions. Though we have built some early prototypes with this construction, these new valves have yet to be fully characterized — this is an area of future work.

⁴<https://www.theleeco.com/products/electro-fluidic-systems/manifold-technology/>

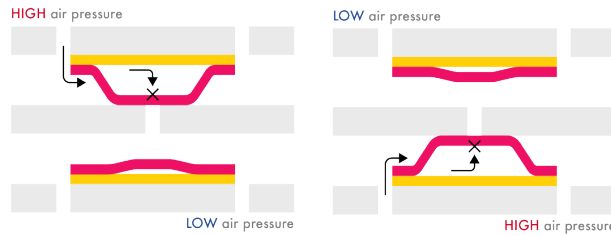


Fig. 23. Concept for a bidirectional Stoma-Board valve, consisting of an upper and lower membrane (two switchable flap valves, back to back). Such a construction resists both positive and negative pressures.

8.5 Stoma-Board as a Raw Material

Ultimately, we envision programmable surfaces that can function as "raw materials" (i.e. available for broad use by designers, not necessarily engineered for one particular application). An LED strip, for example, can be purchased, cut, and applied to an object – in the hands of a user, it is closer to a roll of decorative tape than a flexible circuit board. Such a future may be possible for tactile programmable materials as well, but not within the constraints of a module-driven design.

We see the four characteristics of these layer-driven programmable surfaces (outlined in Section 1) as branching points for subsequent research. For instance, while cell communication within Stoma-Board is neighbor-to-neighbor, the original messages are still generated upstream – a truly information-responsive material could perform this act internally. Future implementations might benefit from a transition towards fully distributed computation. Onboard pressure sources, such as electrostatic or piezoelectric micropumps, can also bring this closer to becoming a fully untethered programmable material.

9 CONCLUSION

We observe that a layer-driven fabrication process, characterized by patterning and stacking, can give rise to programmable surfaces that may scale more readily than their module-driven counterparts. Instead of building and assembling actuators individually, actuators in our framework are formed all at once, during the layup process. The resulting cells are composite mesostructures, cross-sections of which are distributed across the functional layers of our material.

We introduce Stoma-Board as a programmable surface that exemplifies this model. In this particular implementation, the actuator cells are electrostatic valves, which communicate digitally with their neighbors, and regulate the flow of air between a pneumatic transducer layer and a global reservoir. The valves themselves are a novel structure that can resist human-scale pressures of 80 kPa (an order of magnitude larger than earlier variants). As the cells are ultimately responsive to information sources upstream, we are able to use Stoma-Board as a "raw material" to construct several dynamic, pneumatically-powered devices.

Moving forward, research in discretely-actuated programmable surfaces may benefit from this layer-driven lens, adopting composite fabrication techniques and distributed computation paradigms from materials science and robotics.

ACKNOWLEDGMENTS

The authors thank Alexandra Ion, whose comments and feedback improved this work.

REFERENCES

- [1] Jason Alexander, Anne Roudaut, Jürgen Steimle, Kasper Hornbæk, Miguel Bruns Alonso, Sean Follmer, and Timothy Merritt. 2018. Grand challenges in shape-changing interface research. In *Proceedings of the 2018 CHI Conference on Human Factors in Computing Systems*. 1–14.
- [2] Amir Ali Amiri Moghadam, Seyedhamidreza Alaie, Suborna Deb Nath, Mahdie Aghasizade Shaarbafe, James K Min, Simon Dunham, and Bobak Mosadegh. 2018. Laser cutting as a rapid method for fabricating thin soft pneumatic actuators and robots. *Soft robotics* 5, 4 (2018), 443–451.
- [3] Douglas Anjewierden, Gregory A Liddiard, and Bruce K Gale. 2012. An electrostatic microvalve for pneumatic control of microfluidic systems. *Journal of Micromechanics and Microengineering* 22, 2 (2012), 025019.
- [4] Byunghoon Bae, Jaehyeong Han, Richard I Masel, and Mark A Shannon. 2007. A bidirectional electrostatic microvalve with microsecond switching performance. *Journal of Microelectromechanical Systems* 16, 6 (2007), 1461–1471.
- [5] Bavani Balakrishnan, Alek Nacev, and Elisabeth Smela. 2015. Design of bending multi-layer electroactive polymer actuators. *Smart Materials and Structures* 24, 4 (2015), 045032.
- [6] Nadine Besse, Samuel Rosset, Juan Jose Zarate, Elisabetta Ferrari, Luca Brayda, and Herbert Shea. 2017. Understanding graphics on a scalable latching assistive haptic display using a shape memory polymer membrane. *IEEE transactions on haptics* 11, 1 (2017), 30–38.
- [7] Nadine Besse, Samuel Rosset, Juan Jose Zarate, and Herbert Shea. 2017. Flexible active skin: large reconfigurable arrays of individually addressed shape memory polymer actuators. *Advanced Materials Technologies* 2, 10 (2017), 1700102.
- [8] David K Biegelsen, Andrew A Berlin, Patrick Cheung, Mark PJ Fromherz, David Goldberg, Warren B Jackson, Bryan Preas, James Reich, and Lars E Swartz. 2000. AirJet paper mover: An example of mesoscale MEMS. In *Micromachined Devices and Components VI*, Vol. 4176. International Society for Optics and Photonics, 122–129.
- [9] Stuart Diller, Carmel Majidi, and Steven H Collins. 2016. A lightweight, low-power electroadhesive clutch and spring for exoskeleton actuation. In *2016 IEEE International Conference on Robotics and Automation (ICRA)*. IEEE, 682–689.
- [10] Dylan Drotman, Michael Ishida, Saurabh Jadhav, and Michael T Tolley. 2018. Application-driven design of soft, 3-D printed, pneumatic actuators with bellows. *IEEE/ASME Transactions on Mechatronics* 24, 1 (2018), 78–87.
- [11] Juri Fujii, Takuya Matsunobu, and Yasuaki Kakehi. 2018. Colorise: Shape-and color-changing pixels with inflatable elastomers and interactions. In *Proceedings of the Twelfth International Conference on Tangible, Embedded, and Embodied Interaction*. 199–204.
- [12] Jianzhe Gu, David E Breen, Jenny Hu, Lifeng Zhu, Ye Tao, Tyson Van de Zande, Guanyun Wang, Yongjie Jessica Zhang, and Lining Yao. 2019. Geodesy: Self-rising 2.5 D Tiles by Printing along 2D Geodesic Closed Path. In *Proceedings of the 2019 CHI Conference on Human Factors in Computing Systems*. 1–10.
- [13] Hermes Hernandez, Enrique Preza, and Ramiro Velazquez. 2009. Characterization of a Piezoelectric Ultrasonic Linear Motor for Braille Displays. In *2009 Electronics, Robotics and Automotive Mechanics Conference (CERMA)*. 402–407. <https://doi.org/10.1109/CERMA.2009.82>
- [14] Ronan Hinchet, Velko Vechev, Herbert Shea, and Otmar Hilliges. 2018. Dextres: Wearable haptic feedback for grasping in vr via a thin form-factor electrostatic brake. In *Proceedings of the 31st Annual ACM Symposium on User Interface Software and Technology*. 901–912.
- [15] J Blake Jeans and Dennis Hong. 2009. IMPASS: Intelligent mobility platform with active spoke system. In *2009 IEEE International Conference on Robotics and Automation*. IEEE, 1605–1606.
- [16] Clyde F. Coombs Jr. and Happy T. Holden. 2016. *Printed Circuits Handbook, Seventh Edition*. McGraw-Hill Professional.
- [17] T. Kalisky, Y. Wang, B. Shih, D. Drotman, S. Jadhav, E. Aronoff-Spencer, and M. T. Tolley. 2017. Differential pressure control of 3D printed soft fluidic actuators. In *2017 IEEE/RSJ International Conference on Intelligent Robots and Systems (IROS)*. 6207–6213. <https://doi.org/10.1109/IROS.2017.8206523>
- [18] Mustafa Emre Karagozler, Jason D Campbell, Gary K Fedder, Seth Copen Goldstein, Michael Philetus Weller, and Byung Woo Yoon. 2007. Electrostatic latching for inter-module adhesion, power transfer, and communication in modular robots. In *2007 IEEE/RSJ International Conference on Intelligent Robots and Systems*. IEEE, 2779–2786.
- [19] Junji Kawamoto and Fumihiko Asano. 2012. Active viscoelastic-legged rimless wheel with upper body and its adaptability to irregular terrain. In *2012 IEEE/RSJ International Conference on Intelligent Robots and Systems*. IEEE, 157–162.
- [20] Nicholas Kellaris, Vidyacharan Gopaluni Venkata, Garrett M Smith, Shane K Mitchell, and Christoph Keplinger. 2018. Peano-HASEL actuators: Muscle-mimetic, electrohydraulic transducers that linearly contract on activation. *Science Robotics* 3, 14 (2018), eaar3276.
- [21] Joonyeong Kim, Byung-Kil Han, Dongbum Pyo, Semin Ryu, Hanbyeol Kim, and Dong-Soo Kwon. 2020. Braille display for portable device using flip-latch structured electromagnetic actuator. *IEEE transactions on haptics* 13, 1 (2020), 59–65.
- [22] Christopher Kopic and Kristian Gohlke. 2016. Inflatibits: A Modular Soft Robotic Construction Kit for Children. In *Proceedings of the TEF'16: Tenth International Conference on Tangible, Embedded, and Embodied Interaction*. 723–728.
- [23] M Koutsourelis, L Michalas, and G Papaioannou. 2012. Advanced dielectric charging characterization in capacitive MEMS. In *2012 IEEE International Conference on Industrial Technology*. IEEE, 545–550.
- [24] Doug Laney and Dennis Hong. 2005. Kinematic analysis of a novel rimless wheel with independently actuated spokes. In *International Design Engineering Technical Conferences and Computers and Information in Engineering Conference*, Vol. 47446. 609–614.

- [25] Christina Larson, B Peele, S Li, S Robinson, M Totaro, L Beccai, B Mazzolai, and R Shepherd. 2016. Highly stretchable electroluminescent skin for optical signaling and tactile sensing. *science* 351, 6277 (2016), 1071–1074.
- [26] Susan J Lederman and Roberta L Klatzky. 2009. Haptic perception: A tutorial. *Attention, Perception, & Psychophysics* 71, 7 (2009), 1439–1459.
- [27] Daniel Leithinger, Sean Follmer, Alex Olwal, and Hiroshi Ishii. 2015. Shape displays: Spatial interaction with dynamic physical form. *IEEE computer graphics and applications* 35, 5 (2015), 5–11.
- [28] Edouard Leroy, Ronan Hinchet, and Herbert Shea. 2020. Multimode hydraulically amplified electrostatic actuators for wearable haptics. *Advanced Materials* 32, 36 (2020), 2002564.
- [29] Andrew D Marchese, Robert K Katschmann, and Daniela Rus. 2015. A recipe for soft fluidic elastomer robots. *Soft robotics* 2, 1 (2015), 7–25.
- [30] Elena Márquez Segura, James Fey, Ella Dagan, Samvid Niravbhai Jhaveri, Jared Pettitt, Miguel Flores, and Katherine Isbister. 2018. Designing Future Social Wearables with Live Action Role Play (Larp) Designers. In *Proceedings of the 2018 CHI Conference on Human Factors in Computing Systems*. 1–14.
- [31] Hayley McClintock, Fatma Zeynep Temel, Neel Doshi, Je-sung Koh, and Robert J Wood. 2018. The milliDelta: A high-bandwidth, high-precision, millimeter-scale Delta robot. *Science Robotics* 3, 14 (2018).
- [32] Michael Andy McEvoy and Nikolaus Correll. 2018. Shape-changing materials using variable stiffness and distributed control. *Soft robotics* 5, 6 (2018), 737–747.
- [33] Stefano Mintchev, Marco Salerno, Alexandre Cherpillod, Simone Scaduto, and Jamie Paik. 2019. A portable three-degrees-of-freedom force feedback origami robot for human–robot interactions. *Nature Machine Intelligence* 1, 12 (2019), 584–593.
- [34] Shane K Mitchell, Xingrui Wang, Eric Acome, Trent Martin, Khoi Ly, Nicholas Kellaris, Vidyacharan Gopaluni Venkata, and Christoph Keplinger. 2019. An Easy-to-Implement Toolkit to Create Versatile and High-Performance HASEL Actuators for Untethered Soft Robots. *Advanced Science* 6, 14 (2019), 1900178.
- [35] Fuka Nojiri and Yasuaki Kakehi. 2014. BelliesWave: color and shape changing pixels using bilayer rubber membranes. In *ACM SIGGRAPH 2014 Posters*. 1–1.
- [36] Sile O’Modhrain. 2014. Rekindling the search for the Holy Braille. In *2014 IEEE Haptics Symposium (HAPTICS)*. IEEE, xviii–xviii.
- [37] Jifei Ou, Felix Heibeck, and Hiroshi Ishii. 2016. TEI 2016 Studio: Inflated Curiosity. In *Proceedings of the TEI’16: Tenth International Conference on Tangible, Embedded, and Embodied Interaction*. 766–769.
- [38] James Patten and Hiroshi Ishii. 2007. Mechanical constraints as computational constraints in tabletop tangible interfaces. In *Proceedings of the SIGCHI conference on Human factors in computing systems*. 809–818.
- [39] Ron Pelrine, Annjoe Wong-Foy, Brian McCoy, Dennis Holeman, Rich Mahoney, Greg Myers, Jim Herson, and Tom Low. 2012. Diamagnetically levitated robots: An approach to massively parallel robotic systems with unusual motion properties. In *2012 IEEE International Conference on Robotics and Automation*. IEEE, 739–744.
- [40] Panagiotis Polygerinos, Nikolaus Correll, Stephen A Morin, Bobak Mosadegh, Cagdas D Onal, Kirstin Petersen, Matteo Cianchetti, Michael T Tolley, and Robert F Shepherd. 2017. Soft robotics: Review of fluid-driven intrinsically soft devices; manufacturing, sensing, control, and applications in human-robot interaction. *Advanced Engineering Materials* 19, 12 (2017), 1700016.
- [41] Jin-Yuan Qian, Cong-Wei Hou, Xiao-Juan Li, and Zhi-Jiang Jin. 2020. Actuation Mechanism of Microvalves: A Review. *Micromachines* 11, 2 (2020), 172.
- [42] Yu Qiu, Zhiyun Lu, and Qibing Pei. 2018. Refreshable tactile display based on a bistable electroactive polymer and a stretchable serpentine Joule heating electrode. *ACS applied materials & interfaces* 10, 29 (2018), 24807–24815.
- [43] Dan Raviv, Wei Zhao, Carrie McKnelly, Athina Papadopoulou, Achuta Kadambi, Boxin Shi, Shai Hirsch, Daniel Dikovskiy, Michael Zyacki, Carlos Olguin, et al. 2014. Active printed materials for complex self-evolving deformations. *Scientific reports* 4 (2014), 7422.
- [44] Matthew A Robertson, Masato Murakami, Wyatt Felt, and Jamie Paik. 2018. A Compact Modular Soft Surface With Reconfigurable Shape and Stiffness. *IEEE/ASME Transactions on Mechatronics* 24, 1 (2018), 16–24.
- [45] Matthew A Robertson and Jamie Paik. 2017. New soft robots really suck: Vacuum-powered systems empower diverse capabilities. *Science Robotics* 2, 9 (2017).
- [46] Philipp Rothmund, Alar Ainla, Lee Belding, Daniel J Preston, Sarah Kurihara, Zhigang Suo, and George M Whitesides. 2018. A soft, bistable valve for autonomous control of soft actuators. *Science Robotics* 3, 16 (2018).
- [47] Daniela Rus and Michael T Tolley. 2018. Design, fabrication and control of origami robots. *Nature Reviews Materials* 3, 6 (2018), 101–112.
- [48] Alexander Russomanno, Sile O’Modhrain, R Brent Gillespie, and Matthew WM Rodger. 2015. Refreshing refreshable braille displays. *IEEE transactions on haptics* 8, 3 (2015), 287–297.
- [49] Alex Russomanno, Zhentao Xu, Sile O’Modhrain, and Brent Gillespie. 2017. A pneu shape display: Physical buttons with programmable touch response. In *2017 IEEE World Haptics Conference (WHC)*. IEEE, 641–646.
- [50] Deepak Ranjan Sahoo, Timothy Neate, Yutaka Tokuda, Jennifer Pearson, Simon Robinson, Sriram Subramanian, and Matt Jones. 2018. Tangible drops: a visio-tactile display using actuated liquid-metal droplets. In *Proceedings of the 2018 CHI Conference on Human Factors in Computing Systems*. 1–14.

- [51] Sebastian Sanchez and Pranav A Bhounsule. 2021. Design, Modeling, and Control of a Differential Drive Rimless Wheel That Can Move Straight and Turn. *Automation* 2, 3 (2021), 98–115.
- [52] Kazuo Sato and Mitsuhiro Shikida. 1994. An electrostatically actuated gas valve with an S-shaped film element. *Journal of micromechanics and microengineering* 4, 4 (1994), 205.
- [53] Ali Shtarbanov. 2021. FlowIO Development Platform—the Pneumatic “Raspberry Pi” for Soft Robotics. In *Extended Abstracts of the 2021 CHI Conference on Human Factors in Computing Systems*. 1–6.
- [54] Alexa F Siu, Eric J Gonzalez, Shenli Yuan, Jason B Ginsberg, and Sean Follmer. 2018. Shapeshift: 2D spatial manipulation and self-actuation of tabletop shape displays for tangible and haptic interaction. In *Proceedings of the 2018 CHI Conference on Human Factors in Computing Systems*. 1–13.
- [55] Vern Solberg. 2015. Embedding passive and active components: PCB design and fabrication process variations. *IPC APEX EXPO* (2015).
- [56] Pratheev S Sreetharan, John P Whitney, Mark D Strauss, and Robert J Wood. 2012. Monolithic fabrication of millimeter-scale machines. *Journal of Micromechanics and Microengineering* 22, 5 (2012), 055027.
- [57] Miriam Sturdee. 2018. *Sketching as a support mechanism for the design and development of shape-changing interfaces*. Lancaster University (United Kingdom).
- [58] Ryo Suzuki, Jun Kato, Mark D Gross, and Tom Yeh. 2018. Reactile: Programming swarm user interfaces through direct physical manipulation. In *Proceedings of the 2018 CHI Conference on Human Factors in Computing Systems*. 1–13.
- [59] Ryo Suzuki, Ryosuke Nakayama, Dan Liu, Yasuaki Kakehi, Mark D Gross, and Daniel Leithinger. 2020. LiftTiles: constructive building blocks for prototyping room-scale shape-changing interfaces. In *Proceedings of the Fourteenth International Conference on Tangible, Embedded, and Embodied Interaction*. 143–151.
- [60] Yichao Tang, Yanbin Li, Yaoye Hong, Shu Yang, and Jie Yin. 2019. Programmable active kirigami metasheets with more freedom of actuation. *Proceedings of the National Academy of Sciences* 116, 52 (2019), 26407–26413.
- [61] Shan-Yuan Teng, Cheng-Lung Lin, Chi-huan Chiang, Tzu-Sheng Kuo, Liwei Chan, Da-Yuan Huang, and Bing-Yu Chen. 2019. Tilepop: Tile-type pop-up prop for virtual reality. In *Proceedings of the 32nd Annual ACM Symposium on User Interface Software and Technology*. 639–649.
- [62] Joshua D Tice, Amit V Desai, Thomas A Bassett, Christopher A Applett, and Paul JA Kenis. 2014. Control of pressure-driven components in integrated microfluidic devices using an on-chip electrostatic microvalve. *RSC Advances* 4, 93 (2014), 51593–51602.
- [63] Markku Tilli et al. 2015. *Handbook of Silicon Based MEMS Materials and Technologies* (second ed.). William Andrew Publishing, Boston. <https://doi.org/10.1016/B978-0-323-29965-7.00046-4>
- [64] Guanyun Wang, Humphrey Yang, Zeyu Yan, Nurcan Gecer Ulu, Ye Tao, Jianzhe Gu, Levent Burak Kara, and Lining Yao. 2018. 4DMesh: 4D printing morphing non-developable mesh surfaces. In *Proceedings of the 31st Annual ACM Symposium on User Interface Software and Technology*. 623–635.
- [65] Malte Weiss, Florian Schwarz, Simon Jakubowski, and Jan Borchers. 2010. Madgets: actuating widgets on interactive tabletops. In *Proceedings of the 23rd annual ACM symposium on User interface software and technology*. 293–302.
- [66] Yichuan Wu, Justin K Yim, Jiaming Liang, Zhichun Shao, Mingjing Qi, Junwen Zhong, Zihao Luo, Xiaojun Yan, Min Zhang, Xiaohao Wang, et al. 2019. Insect-scale fast moving and ultrarobust soft robot. *Science Robotics* 4, 32 (2019).
- [67] Kazushi Yoshida, Shuji Tanaka, Yosuke Hagihara, Shigeaki Tomonari, and Masayoshi Esashi. 2010. Normally closed electrostatic microvalve with pressure balance mechanism for portable fuel cell application. *Sensors and Actuators A: Physical* 157, 2 (2010), 290–298.
- [68] Shigeo Yoshida, Yuqian Sun, and Hideaki Kuzuoka. 2020. PoCoPo: Handheld pin-based shape display for haptic rendering in virtual reality. In *Proceedings of the 2020 CHI Conference on Human Factors in Computing Systems*. 1–13.
- [69] Juan Jose Zarate, Olexandr Gudozhnik, Anthony Sébastien Ruch, and Herbert Shea. 2017. Keep in touch: portable haptic display with 192 high speed taxels. In *Proceedings of the 2017 CHI Conference Extended Abstracts on Human Factors in Computing Systems*. 349–352.
- [70] Juan José Zárate and Herbert Shea. 2016. Using pot-magnets to enable stable and scalable electromagnetic tactile displays. *IEEE transactions on haptics* 10, 1 (2016), 106–112.
- [71] Kai Zhang, Eric J Gonzalez, Jianglong Guo, and Sean Follmer. 2019. Design and Analysis of High-Resolution Electrostatic Adhesive Brakes Towards Static Refreshable 2.5 D Tactile Shape Display. *IEEE Transactions on Haptics* 12, 4 (2019), 470–482.
- [72] Wen-Ming Zhang, Han Yan, Zhi-Ke Peng, and Guang Meng. 2014. Electrostatic pull-in instability in MEMS/NEMS: A review. *Sensors and Actuators A: Physical* 214 (2014), 187–218.